

Review

Open Access



Recent progress of enhanced bubble separation in alkaline water electrolyzer

Lin Yang¹, Lingyu Gao¹, Guixuan Shan¹, Xinyi Huo¹, Mengfei Zhang¹, Yuxuan Wang¹, Xingyu Liu¹, Aiqun Kong², Jiangjiexing Wu^{3,*} , Jinli Zhang^{1,2,*} 

¹School of Chemical Engineering and Technology, Tianjin University, Tianjin 300350, China.

²School of Chemistry and Chemical Engineering, Shihezi University, Shihezi 832003, Xinjiang, China.

³School of Marine Science and Technology, Tianjin University, Tianjin 300072, China.

*Correspondence to: Dr. Jiangjiexing Wu, School of Marine Science and Technology, Tianjin University, No. 92 Weijin Road, Nankai District, Tianjin 300072, China. E-mail: wjx1987@tju.edu.cn; wujiangjiexing2007@126.com; Prof. Jinli Zhang, School of Chemical Engineering and Technology, Tianjin University, No. 135 Yaguan Road, Haihe Education Park, Tianjin 300350, China. E-mail: zhangjinli@tju.edu.cn

How to cite this article: Yang L, Gao L, Shan G, Huo X, Zhang M, Wang Y, Liu X, Kong A, Wu J, Zhang J. Recent progress of enhanced bubble separation in alkaline water electrolyzer. *Chem Synth* 2023;3:41. <https://dx.doi.org/10.20517/cs.2023.25>

Received: 2 May 2023 **First Decision:** 30 Jun 2023 **Revised:** 30 Jul 2023 **Accepted:** 22 Aug 2023 **Published:** 27 Sep 2023

Academic Editors: Bao-Lian Su, Aicheng Chen **Copy Editor:** Pei-Yun Wang **Production Editor:** Pei-Yun Wang

Abstract

Alkaline water electrolysis has a large industrial application and development potential in hydrogen energy owing to its high maturity and low cost. However, its moderate energy efficiency, especially caused by bubble effects, inhibits its use for large-scale hydrogen production. To overcome this shortcoming, this review first analyzes the bubble effect and summarizes the external operation methods, such as external field intensification, flow operation, fluctuation operation, and surfactant addition to the electrolyte, to enhance bubble separation in the electrolyzer. Then, electrode and flow channel structure optimization, particularly superhydrophilic and superaerophobic electrodes, and flow channels with varying heights, square column arrangements, and inlet/outlet numbers are highlighted. Finally, future research directions in alkaline water electrolysis technology are suggested to advance the industrial application of large-scale alkaline water electrolysis.

Keywords: Alkaline water electrolyzer, bubble effect, external operation optimization, superhydrophilic and superaerophobic electrode, bipolar plates flow channel



© The Author(s) 2023. **Open Access** This article is licensed under a Creative Commons Attribution 4.0 International License (<https://creativecommons.org/licenses/by/4.0/>), which permits unrestricted use, sharing, adaptation, distribution and reproduction in any medium or format, for any purpose, even commercially, as long as you give appropriate credit to the original author(s) and the source, provide a link to the Creative Commons license, and indicate if changes were made.



INTRODUCTION

Hydrogen energy plays a key role in the transition to a zero-carbon energy system that is cleaner, more sustainable, and lower in emissions. As a raw material for industrial production, hydrogen is widely used for oil refining, ammonia synthesis, methanol synthesis, and other chemical processes^[1]. Among the total hydrogen production in the world, hydrogen electrolysis accounts for only 4% due to its higher cost than fossil fuels. Nevertheless, electrolysis can reduce the cost of electrolytic water to hydrogen since it adapts to the discontinuous and unstable power supply characteristic of renewable energy systems, including wind, light, and water^[2]. Connecting renewable energy to the grid by controlling the electrolytic water to hydrogen system can reduce the intermittency of renewable energy, integrate multiple energy sectors, and improve energy power system integration^[3]. In this way, hydrogen production by electrolysis of water has received increasing attention.

An electrolyzer is the main production equipment of electrolytic water, which can be divided into three categories according to the electrolyte, namely alkaline water electrolyzers (AWEs), proton exchange membrane water electrolyzers (PEMWEs), and solid oxide electrolysis cells (SOECs). In terms of energy efficiency, the SOEC operating at 650-1000 °C has the highest efficiency, but it is still in the development phase^[4]. As of now, both AWEs and PEMWEs are commercially available. PEMWEs have advantages in terms of operating pressures, load ranges, and footprints, while AWEs are more cost-effective, have larger equipment sizes, and have a longer lifetime. In particular, the single unit product size of AWEs (MW scale) is larger than that of PEMWEs (kW scale); the cost of AWEs is about half that of PEMWEs, and AWEs last up to twice as long as PEMWEs. A comparison of the three water electrolysis technologies is shown in [Table 1](#). Together, alkaline water electrolysis has greater industrial applicability and development potential due to its high maturity and low cost and will continue to be the mainstream technology^[5]. The development of advanced nanomaterials has provided new opportunities to enhance the performance of AWEs. Nanomaterials, such as metal nanoparticles and carbon nanotubes, have been shown to improve electrode kinetics and catalytic activity when incorporated into electrolyzer components. A nanoscale surface area, electrical conductivity, and other beneficial properties are responsible for this. Developing and optimizing nanomaterial-modified electrodes have become an active area of research to improve alkaline water electrolysis efficiency, durability, and cost-effectiveness, resulting in significant improvements in electrolyzer performance.

Despite its remarkable success, alkaline water electrolysis still faces some bottlenecks, such as energy inefficiency^[6]. One of the biggest reasons for energy inefficiency is bubbles, which produce high overpotentials and large ohmic voltage drops when they generate, cover, or disperse in the electrolyte^[7-9]. Hence, it is important to eliminate bubble effects, and numerous studies have been undertaken to do so. To highlight the progress of bubble elimination, this review first discusses the bubble effect and external methods to aid bubble separation, such as adding external fields, flow operation, fluctuating operation, and adding surfactants to the electrolyte. Following that, two key electrolyzer structures, electrodes and flow channels, are described to eliminate the bubble effect. Lastly, we discuss the perspectives that may lead to future advancements in alkaline water electrolysis.

BUBBLE EFFECT

During the electrolysis of water, gas bubbles are produced at the interface of three phases: gas, liquid, and solid^[8]. However, these bubbles negatively affect electrolysis performance, which is referred to as the bubble effect and is associated with two main effects^[10]. One is the screening effect, in which the electrolyte is expelled from the electrode surface by bubbles, resulting in an increase in local current densities. The other is the void effect, which implies longer ion transport pathways and lower electrolyte conductivity due to the presence of bubbles.

Table 1. Comparison of different water electrolysis technologies for producing hydrogen

	AWE	PEMWE	SOEC
Electrolyte	20-30 wt% KOH	PEM	Y ₂ O ₃ /ZrO ₂
Operating temperature (°C)	60-95	50-80	600-1,000
Current density (A·cm ⁻²)	0.15-0.65	1.00-2.00	0.20-1.00
Electrolysis efficiency (%)	60-75	70-90	85-100
System efficiency (%)	51-60	46-60	76-81
Electrolyzer energy consumption (kW·h·Nm ⁻³)	4.20-4.80	3.80-5.00	2.60-3.60
System energy consumption (kW·h·Nm ⁻³)	5.00-5.90	5.20-5.90	3.70-3.90
Load elasticity (%)	20-100	0-120	-100-100
Cold start time	1-2 h	5-10 min	> 1 h
Warm start time	1-5 min	< 5 s	15 min
Industrialization operation pressure (MPa)	0.10-3	0.10-5	0.10-1.50
Scientific research operation pressure (MPa)	0.10-10	0.10-70	0.10-1.50
Operation and maintenance	Complex and high cost	Simple and low cost	Mainly for experimental research
Commercial features	Mature, industrial, low investment	Small-scale application, high investment	Experimental stage, not industrialized

AWE: Alkaline water electrolysis; PEMWE: proton exchange membrane water electrolysis; SOEC: solid oxide electrolysis cell.

During water electrolysis, bubbles first form and adhere to electrode surfaces, and only once they reach a critical size can they be separated from the electrode surfaces. In specific terms, the evolution of bubbles involves nucleation, growth, and detachment^[11]. By electrolysis, hydrogen or oxygen molecules are generated around the electrode where they reach a critical nucleation concentration at which bubbles will nucleate and adhere to the electrode. The screening effect occurs when adhering bubbles cover the active sites of the electrode, impeding contact between the electrode and the electrolyte^[9]. Additionally, adhering bubbles cause ion transport to be impeded, which leads to the void effect^[12]. The screening effect and void effect increase as the bubbles grow larger, which leads to local overpotential increase as well. When a critical size is reached, bubbles will detach from electrode surfaces, resulting in a gradual decrease in the contact area between bubbles and electrodes, a weakening of the screening effect, and a reduction in local overpotential. In the course of detachment, the bubbles will end up as free bubbles in the electrolyte, and the void effect of these free bubbles will have an obvious effect on the electrolysis process. Notably, these free bubbles may also come into contact with or slip along the electrode surface during the flow process, thus generating the screening effect^[13]. The combined negative effects of the bubble effect inevitably increase the energy consumption of the electrolytic water. Moreover, the energy efficiency reduction caused by the bubble effect is exacerbated at higher current densities.

According to [Figure 1](#), the force analysis of the bubble on the electrode surface shows that the bubble is mainly affected by the upward buoyancy force F_b and the downward adhesion force F_a (gravity cannot be ignored), described by the following two Equations (1)-(2), respectively^[14].

$$F_a = 2\pi\gamma R_b \sin\theta = \gamma 2\pi(R \sin\theta) \sin\theta \quad (1)$$

$$F_b = \frac{4}{3}\pi R^3 \rho g \quad (2)$$

where R is the bubble radius, R_b is the radius of the inactive area, θ is the bubble-electrode contact angle, ρ is the electrolyte density, and γ is the electrode surface tension. In the case where $F_b = F_a$, R is related to θ through the following relationship Equation (3):

$$R \propto \sqrt{\gamma} \sin\theta \quad (3)$$

According to the above equations, the size of the bubble leaving the electrode surface corresponds to the force of bubble adhesion F_a . The bubble adhesion force can be reduced by reducing the contact angle and electrolyte surface tension, allowing the bubbles to leave the electrode surface quickly and with a very small volume. When the bubble volume leaving the electrode surface is smaller, the bubble stays on the electrode for a shorter period; the bubble coverage is smaller, and the bubble effect is less noticeable on the electrode.

Furthermore, bubbles separated from the electrode and dispersed in the electrolyte will occupy the effective volume of the electrolyte, increasing its ion migration resistance and, therefore, increasing its ohmic overpotential. Bruggeman equation^[15] states that the electrolyte conductivity σ_e ($\text{S}\cdot\text{m}^{-1}$) depends on gas volume fraction Φ_g and is given by:

$$\sigma_e = \sigma_0 \times (1 - \Phi_g)^{1.5} \quad (4)$$

where σ_0 ($\text{S}\cdot\text{m}^{-1}$) is the conductivity of the electrolyte without the influence of the gas. Clearly, the more uniform the distribution of bubbles in the electrolyte, the less effect it has on the conductivity. Thus, it is an effective method for reducing the ohmic overpotential of electrolytes by ensuring uniform bubble distributions.

IMPROVEMENTS TO EXTERNAL OPERATIONS

Based on the above analysis, external operation enhancements are applied to speed up the separation of bubbles from electrode surfaces, reducing bubble-induced energy loss. Following is a description of the specific methods, including the addition of external fields, flow operation, fluctuating operation, and adding surfactants to the electrolyte.

External fields

When external field enhancement is added to the water electrolysis process, the bubble separation process is accelerated, and the total system resistance is reduced, thus reducing energy consumption^[16]. In most cases, the electrolyzer is enhanced by a magnetic field, since obtaining a stable magnetic field is easier, and introducing such a field is as simple as placing the electrode between magnets. The magnetohydrodynamic force (Lorentz force) enhances electrochemical performance as it aligns with bubble buoyancy to improve bubble escape, reduce ohmic polarization, and increase current densities [Figure 2A]^[17-19]. In addition, magnetothermal effects^[20] and electron spin selectivity^[21] could also contribute to hydrolysis through

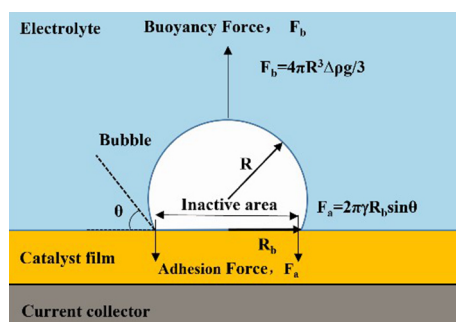


Figure 1. Force analysis of the bubble. Force analysis of a single gas bubble sitting on the catalyst film suffers two main forces: buoyant force (F_b) and adhesion force (F_a). This figure is quoted with permission from Lu et al.^[14].

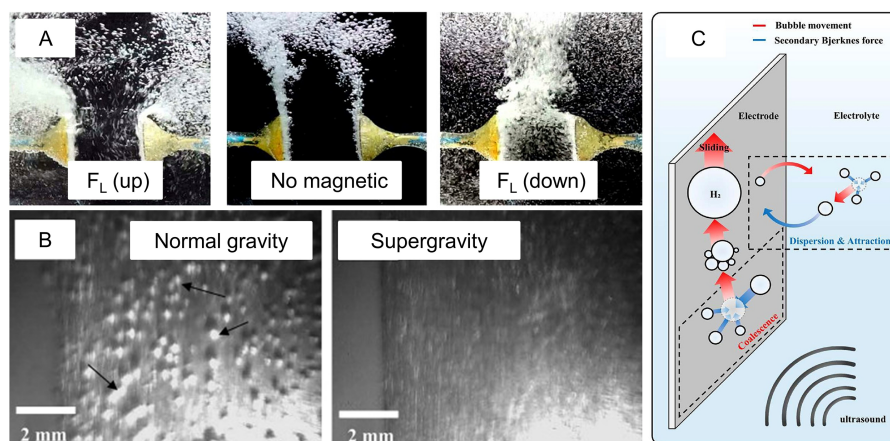


Figure 2. Effects of external field enhancement on bubble separation^[18,22,25]. (A) convection created by magnetic fields of different directions, voltage: 4 V, electrode distance: 10 mm, KOH: 40 wt%, magnetic field intensity: 4.5 T. These figures are quoted with permission from Martin^[18]; (B) the photograph of the electrode surface during a hydrogen bubble evolution process at $0.05 \text{ A}\cdot\text{cm}^{-2}$ with normal gravity conditions and supergravity fields. These figures are quoted with permission from Wang et al.^[22]; (C) a mechanism of bubble elimination in ultrasonic fields. This figure is quoted with permission from Cho et al.^[25].

magnetic fields. In spite of this, magnetic field enhancement has some limitations, such as low field strength and high energy input, which prevent its further application on an industrial scale.

Separation processes involving multiphase systems can also be accelerated by supergravity fields. In water electrolysis, supergravity fields can enhance gas-liquid phase separation and interphase slip velocity, resulting in less bubble coverage on the catalyst surface and more hydrogen production [Figure 2B]^[22,23]. It was estimated that water electrolysis would save 9%-17% of energy at $0.5 \text{ A}\cdot\text{cm}^{-2}$. Cavitation, an effect of ultrasonic fields, can be very significant in separating bubbles as well^[24]. Cavitation bubbles rupture periodically, causing hydrogen or oxygen bubbles to accelerate from the electrode surface and electrolyte due to the violent stirring effect, which speeds up mass transfer on the electrode [Figure 2C]^[25]. Moreover, the ultrasonic field reduces reaction overpotential through additional free radical production^[26]. The supergravity fields and ultrasonic fields, however, may require large investments in industrial electrolysis equipment and cause significant damage^[27].

Flow

A flow-through operation was found to be effective for removing bubbles from electrode surfaces. In contrast to conventional planar static electrodes, flow electrodes use forced liquid flow orthogonal to the

porous catalyst electrode surface^[28]. By doing so, adhering bubbles may be removed from the catalyst surface, especially at high current densities, and losses caused by kinetic overpotentials and ohmic resistance would be reduced^[13,29]. According to the report by Fan^[30], a flow field can reduce the cell voltage from 2.92 to 2.78 V at 1,000 mA·cm⁻², which reduces the corresponding consumption by about 0.55 kW·h·Nm⁻³. Nevertheless, increasing the flow rate can only improve the performance of an electrolyzer in a limited way. When the flow rate increases past a certain threshold, electrolysis performance no longer improves, while the energy usage of the pump continues to increase. Therefore, it is necessary to select an appropriate flow rate according to the structure, scale, and operating conditions of the AWE to maximize its efficiency.

Fluctuations

Fluctuations on the electrode surface can reduce both bubble coverage and concentration polarization. Currently, pressure swings and pulsed power are primarily used to study fluctuations. According to Bakker *et al.*, brief pressure decreases accelerate bubble removal from electrodes and other parts, such as the diaphragm and polar plate, because the bubble size rapidly increases^[31]. For pressure swings from 4 bar to 1 bar applied every 100-300 s in a rectangular electrochemical flow cell experimental rig, the voltage reduction is at most 0.1 V, increasing almost linearly with the current density. A larger electrolytic system, however, requires more pressurization equipment and additional energy to pressurize the entire system.

An alternative pulsed power operation reduces or stops power energization periodically to increase energy efficiency. By pulsing power, the diffusion layer on the electrode surface can be reduced or eliminated, bubbles can leave the electrode surface, and electrode surface reactants can be replenished^[32]. Using a high frequency pulse voltage with a duty cycle, Demir *et al.* significantly increased hydrogen production in an electrochemical water electrolyzer^[33]. A duty cycle of 50% and a frequency of 200 kHz at 6 V reduced energy consumption by 20%-25%. While pulsed electrolysis improves energy efficiency, it does not sufficiently compensate for reduced productivity caused by ceasing current.

Surfactants

When ionic or nonionic surfactants are added, the specific surface energy associated with bubble formation and growth is reduced, resulting in smaller bubbles and reduced bubble adhesion^[34]. Various surfactants, such as cetyltrimethylammonium bromide (CTAB)^[35] and isopropyl alcohol^[36], can also enhance the adsorption of reactant ions at the electrode/electrolyte interface to improve hydrolysis. Surfactants, however, pose a problem. Organic compounds typically undergo oxidation more readily and react at lower potentials compared to water or hydroxides. This can contribute to an increase in the current density and a decrease in potential upon the addition of surfactants. Furthermore, surfactants can form highly stable micro/nano-bubbles or droplets, which can make the separation of gas-liquid phases more difficult. As a result, greater input is required in the subsequent gas-liquid separator and gas scrubber to ensure complete gas-liquid separation.

IMPROVEMENTS TO ELECTROLYZER STRUCTURES

Although external operations can potentially improve bubble separation, there are still limitations, especially when it comes to industrial applications. Therefore, the design optimization of key components of AWEs is crucial for scaling up the technology. In particular, the design optimization of electrodes and bipolar plate flow channels has received significant attention in current research. This is because these components play a crucial role in determining the performance and efficiency of the electrolyzer. By optimizing the design of these components, it is possible to improve the overall performance and reduce the cost of the electrolyzer. This is especially important for large-scale electrolyzers, where even small improvements in efficiency can have a significant impact on the overall cost and feasibility of the

technology.

Electrodes

As the site where the electrolytic reaction occurs, the electrode is a crucial component of an AWE. In electrode optimization, there are two types: structural optimization, where nickel electrodes remain active sites, and property optimization, where nickel electrodes only serve as supports. (Note: Since space is limited, this review will only cover nickel electrodes, which are commonly used in industrial AWEs due to their corrosion resistance, low cost, and high stability^[37]. Although noble metal catalysts such as platinum and palladium can obtain excellent performance in electrolytic water through modulation^[38-40], their application in alkaline electrolytic water is restricted due to factors such as high cost, poor stability, and limited availability compared to nickel electrodes^[41]. In comparison with nickel, graphite and stainless steel are cheaper. However, the lower catalytic activity and corrosion resistance of graphite and the poorer electrical conductivity and polarization of stainless steel make them unsuitable for AWEs, which require long-term stable operation. Additionally, the foam structure will enable a higher reactivity and mass transfer rate, making it more adaptable to the industrial flow zero-gap electrolyzer.)

Structural optimization

To ensure sufficient active sites, fast electrochemical reactions require electrodes with a large surface area. Generally, porous electrodes are able to meet the requirement for a large surface area. Several studies have shown that nickel foam (NF) electrodes with porous structures reduce overpotential and increase current densities in the electrolyzer^[42-44]. In NF, however, a significant amount of bubbles is normally generated, causing significant resistance if the bubbles are not removed in a timely manner^[45,46]. According to Kim *et al.*, the structure of a porous electrode did influence bubble separation from the inside of the electrode^[47]. In [Figure 3A1](#) and [A2](#), there was fabricated an asymmetric NF electrode with different pore structures on each side, one having about 5 μm pores for electrochemical reaction sites and the other having about 100 μm pores for gas/electrolyte separation. On the small pore side of the electrode, hydrogen and oxygen molecules do not form bubbles at first, but they do so after diffusing through the pores to the large pore side, which makes their expulsion easier. A current density close to 0.5 $\text{A}\cdot\text{cm}^{-2}$ was observed in electrochemical tests conducted at 80 $^{\circ}\text{C}$ and 1.8 V, much higher than reported in some literature and commercial devices [[Figure 3B](#)]. The method provides a new approach to optimizing the electrodes for AWEs with zero gaps.

Alternatively, microstructures can be used to meet large surface requirements but allow bubbles to escape as well^[6]. As an example, Paul *et al.* used photolithography to fabricate hexagonal nickel electrode arrays with raised or recessed microstructures that corresponded with the size of oxygen bubbles generated by OER [[Figure 3C1](#) and [C2](#)]^[48]. Compared to a flat nickel electrode, the micro-scale nickel recesses enhance mass transfer and activity, resulting in double the current density, bubble release, and a reduction in reaction overpotential. In [Figure 3D1](#) and [D2](#), a variant of nickel electrodes with micropatterned structures was further investigated by Fujimura *et al.*^[49]. In situ observations of surface bubble behavior, contact angle measurements, and electrochemical measurements [[Figure 3E1](#) and [E2](#)] indicated that micropattern coverage and shape affected the wettability of electrode surfaces, promoting bubble separation.

In addition to the aforementioned studies, researchers have also investigated the use of hydrophobic materials to improve electrode structures in order to control bubble formation and facilitate bubble separation and release^[28,50]. For instance, the use of polytetrafluoroethylene (PTFE) coatings on nickel electrodes has been found to be effective in this regard^[51]. The hydrophobic PTFE surfaces serve as collectors for dissolved gases, while the open nickel surfaces facilitate electrode reactions. From [Figure 3F1-F4](#), by increasing the coverage of PTFE on the surface of the porous nickel electrode, the surface becomes more hydrophobic, which can affect the coverage, size, and kinetics of bubbles that form on the electrode

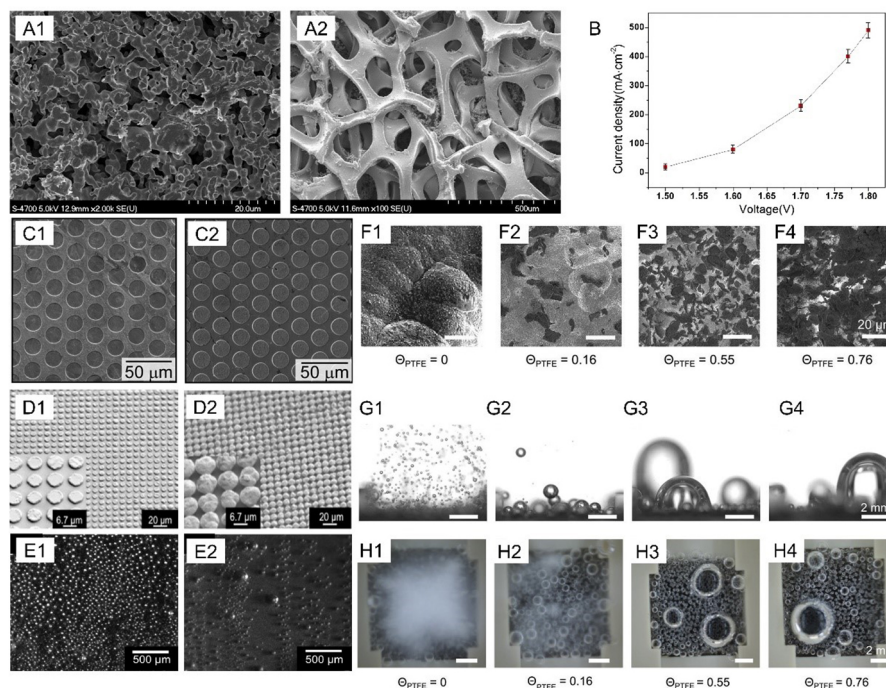


Figure 3. Different methods of electrode structure optimization^[47-50]. SEM pictures of the nickel electrode: (A1) the surface with 5 μm pores; (A2) the other surface with 100 μm pores; (B) the current-voltage curve of the Ni electrodes. These figures are quoted with permission from Kim *et al.*^[47]. SEM images of (C1) an array of 20 μm \varnothing Ni film and (C2) an array of 20 μm \varnothing Ni pillars. These figures are quoted with permission from Paul *et al.*^[48]; Corresponding in situ optical microscope images: (E1) cylindrical Ni microarray, Ni coverage: 39.9%, contact angle: 89.5°; and (E2) semispherical Ni microarray, Ni coverage: 74.7%, contact angle 112.5°. These figures are quoted with permission from Fujimura *et al.*^[49]. SEM images of (F1-F4) the electrodeposited nickel foil and determined the PTFE coverage. (G1-G4) side and (H1-H4) top views of oxygen bubbles corresponding to PTFE coverage in alkaline water splitting experiments performed with porous electrodes. These figures are quoted with permission from Iwata *et al.*^[50]. PTFE: Polytetrafluoroethylene.

surface [Figure 3G1-G4, H1-H4]^[50]. In a 5M KOH electrolyte with a current density of 1,000 mA/cm², 20% PTFE coverage decreased the overpotential from 1.73V to 1.58V^[51]. In addition to PTFE, fluorocarbons have also been conformally deposited to create a hydrophobic pit within an annular microelectrode, resulting in a bubble-free surface^[52]. However, despite their effectiveness in facilitating bubble separation, there is limited research on optimizing electrolytic water electrodes using hydrophobic materials. In light of gas-consumption electrochemical studies using hydrophobic materials to construct hydrophobic electrode interfaces^[53-56], more hydrophobic materials, such as Nafion, polypropylene, polydimethylsiloxane, polyvinylidene fluoride, and fluorinated ethylene propylene, could be investigated to conduct more comprehensive and extensive research into electrolytic water electrodes.

Property optimization

In contrast to the aforementioned strategies, property optimization not only affects the surface structure but also acts as active sites in place of nickel electrodes, with the nickel electrodes serving as support. Previous studies have reported that improvements in the performance of water electrolysis electrodes are mainly achieved by increasing the number of active sites^[57], enhancing the activity strength of these sites^[58,59], and reducing the impact of bubble effects^[60]. Gas bubble adhesion behavior can be flexibly tuned by modifying the electrode surface hydrophilicity and aerophobicity^[60,61]. Some commonly used materials are conductive polymers, graphene and graphene oxide, carbon nanotubes, metal oxides, and hydrogels. These materials can be used alone or in combination to create hydrophilic and aerophobic electrodes. The hydrophilicity

and aerophobicity of electrodes can also be further enhanced with surface treatments, such as plasma treatment or chemical modification. When the contact angle of bubbles is greater than 150° ^[60], i.e., when the material surface reaches superaerophobicity, it can be considered that bubbles can be effectively removed. The connection between the wettability behavior of different solids in water and air is shown in Figure 4. It is also important to note that improving the hydrophilicity of electrode surfaces can enhance the contact between the electrolyte and the catalyst active center, resulting in the more efficient generation of active hydrogen and oxygen reaction intermediates^[62]. Additionally, having an aerophobic electrode surface can promote the rapid formation and release of smaller bubbles, which can prevent blockages of the catalytic active center due to smaller contact angles. These can lead to improved overall performance and efficiency of the alkaline water electrolysis system^[63-66]. Hence, current research on electrode design optimization focuses on developing advanced materials and surface coatings that exhibit these desirable properties.

Lu *et al.* were the first to propose the concept of “superaerophobicity” for electrolytic water electrodes^[60]. In their experiments, the superaerophobic MoS_2 nanosheet array electrodes were synthesized hydrothermally with the electrode substrate made of Ti foil. The bubbles generated on the surface of MoS_2 electrodes with nanoarray structure have discontinuous gas-liquid-solid three-phase contact lines, which promote the bubbles to leave the electrode surface at a later stage and significantly improve the hydrogen evolution reaction (HER) performance.

Then Shan *et al.* prepared a bifunctional CoMoS_x/NF electrocatalyst by in situ metathesis reaction using NF as a substrate^[67]. The hierarchical nanostructures provided the electrode superhydrophilic and superaerophobicity properties, which promote the rapid release of bubbles from the electrode surface [Figure 5A and B]. The catalyst is also abundant with catalytic sites through Co doping and exhibits excellent electrochemical activity and stability at high current densities. As shown in Figure 5C and D, it has a current density of $500 \text{ mA}\cdot\text{cm}^{-2}$ at a low voltage of 1.89 V under alkaline conditions and can maintain its activity without decay for 100 h. It provides a guideline for the development of an efficient catalyst for large-scale water electrolysis.

Up to now, transition metal-based catalysts based on NF electrodes, such as oxides, phosphides, sulfides, carbides, and nitrides, have been widely researched and show high catalytic performance in alkaline water electrolysis. Some recent studies have shown that MXene, as a new type of transition metal carbon/nitride with a two-dimensional structure, possesses richer active sites, larger active surface area, and good hydrophilicity, which can improve the electrode conductivity and electrochemical stability during alkaline water electrolysis, and is a promising electrocatalyst or catalyst carrier.

The poor intrinsic electrocatalytic hydrogen evolution activity of MXene requires surface property modulation or hierarchical structure design of MXene, which can assist in the preparation of highly active and durable hydrogen evolution catalysts. Recently, our group^[68] has prepared superaerophobic $\text{Ru}/\text{c-Ti}_3\text{C}_2/\text{NF}$ 3D electrodes by hydrothermal methods in situ [Figure 6A]. The two-dimensional material MXene (Ti_3C_2) was modified through CTAB (cetyltrimethylammonium bromide) to increase layer spacing and accelerate electron transport, referred to as $\text{c-Ti}_3\text{C}_2$. As a result of the addition of modified $\text{c-Ti}_3\text{C}_2$, the electrode surfaces of $\text{c-Ti}_3\text{C}_2/\text{NF}$ and $\text{Ru}/\text{c-Ti}_3\text{C}_2/\text{NF}$ were almost submerged in water, with a contact angle near zero. Meanwhile, the bubble contact angles of the electrodes were 169° in the superaerophobic range. Therefore, the modified nickel electrodes were considerably improved in terms of hydrophilicity and superaerophobicity [Figure 6B]. The bubble size and bubble release rate on the electrode surface were tracked in situ by a particle imaging velocimetry system and a high-speed framing camera system. As can be seen in Figure 6B, compared to the NF electrode, the bubble size decreased sharply from $300 \mu\text{m}$ to about $60 \mu\text{m}$ after deposition on the NF surface with $\text{c-Ti}_3\text{C}_2$, and the flow field velocity near the electrode

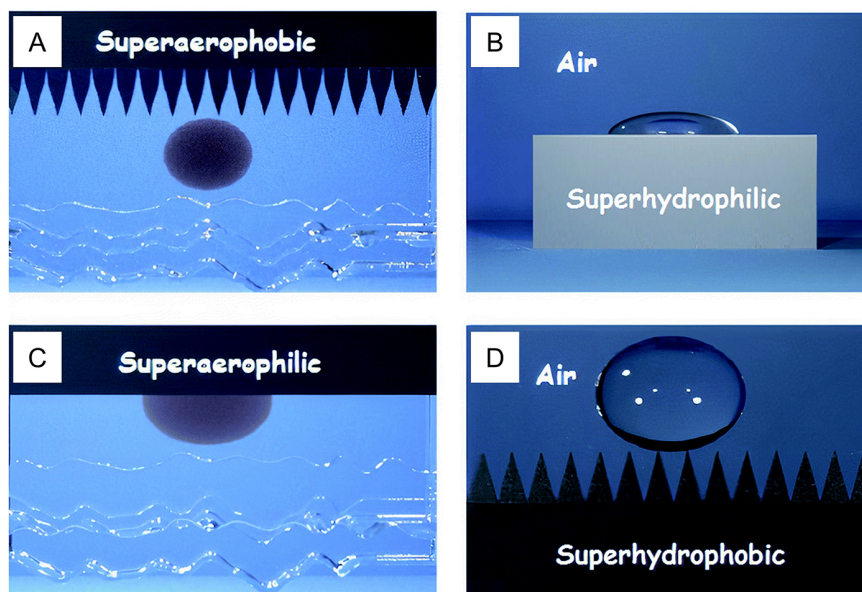


Figure 4. The connection between the wettability behavior of different solids in water and air. (A) Superaerophobic surfaces in water; (B) Superhydrophilic surfaces in air; (C) Superaerophilic surfaces in water; (D) Superhydrophobic surfaces in air. These figures are quoted with permission from Andaveh *et al.*^[66].

increased from $0.8 \text{ mm}\cdot\text{s}^{-1}$ to $3.0 \text{ mm}\cdot\text{s}^{-1}$, while the bubble size on the surface of the prepared Ru/c-Ti₃C₂/NF electrode was only about $40 \text{ }\mu\text{m}$, and the local flow field velocity can reach $7.0 \text{ mm}\cdot\text{s}^{-1}$. The main reason is that due to the introduction of the two-dimensional material c-Ti₃C₂, the superaerophobicity is improved, and bubbles generated by the electrode are rapidly released into the electrolyte. In Figure 6C and D, the overall water splitting test was used for the Ru/c-Ti₃C₂/NF electrode; the cell voltage was only 1.53 V at a current density of $10 \text{ mA}\cdot\text{cm}^{-2}$ and no decay for 20 h, compared with 1.58 V for the commercial Pt-C/NF and RuO₂/NF coupled electrodes. Based on the above results, it is shown that the superhydrophilic and superaerophobic properties of the 3D folded structure of the Ru/c-Ti₃C₂/NF electrode facilitate the wetting of the electrolyte and the timely release of bubbles at high current densities, thus improving the mass transfer of the catalytic electrode and the electrolytic water hydrogen production activity and stability.

It was found that Ru/c-Ti₃C₂/NF 3D electrodes exhibited excellent superhydrophilic performance at low current densities, while the stability of Ru/c-Ti₃C₂/NF electrodes was relatively poor at high current densities ($500 \text{ mA}\cdot\text{cm}^{-2}$). It is mainly because at high current densities, due to the overwhelming reaction, a large number of bubbles will be generated on the electrode surface, leading to catalyst detachment, increased interfacial resistance, and reduced mass transfer efficiency. In order to solve the above problems, the modification process of the electrode surface needs to be improved. Therefore, we enhanced the interaction between the Ti₃C₂ and NF surface using electrodeposition techniques in the next study^[69]. The electrodeposition technology can significantly improve the interaction between the catalytic layer and the conductive substrate, which is beneficial to resist the stress generated by bubble detachment and ensure the stable performance of electrolytic water under high current densities^[70]. Based on previous research, Our group, Kong *et al.*, developed a novel and simple strategy to modulate the interaction between Ti₃C₂ and NF surface using electrodeposition techniques in Figure 7A-C, which can improve the stability of its deposition on the NF surface^[71]. When Ti₃C₂ was electrodeposited, the hydrophilic and aerophobic properties of Ti₃C₂/NF electrodes were improved with a water contact angle and bubble contact angle of 90° and 149° , respectively. By further hydrothermal treatment of Ti₃C₂/NF to form Ni(OH)₂ nanoarrays, the

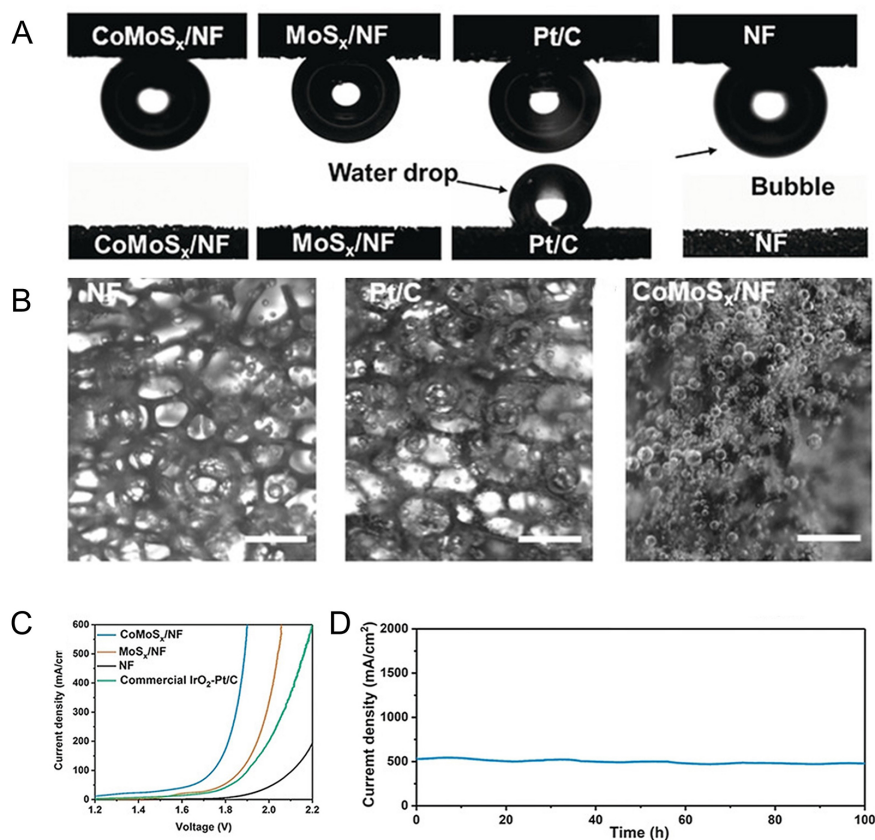


Figure 5. Superhydrophilic/superaerophobic electrocatalyst composed of the supported CoMoS_x Chalco-gel. (A) air-bubble contact angles under water (top) and static-water-droplet contact angles (bottom) for CoMoS_x/NF, MoS_x/NF, Pt/C, and NF; (B) images of bubbles released at the surface of NF, CoMoS_x/NF, and Pt/C for HER at a current density of 200 mA·cm⁻²; (C) and (D) overall water splitting polarization curves of four electrodes and catalytic stability of CoMoS_x/NF. These figures are quoted with permission from Shan et al.^[67]. NF: Nickel foam.

corresponding water contact angle of TiO₂/Ni(OH)₂/NF and Pt/TiO₂/Ni(OH)₂/NF electrodes was close to zero, and the bubble contact angle reached 164° and 171° [Figure 7C], respectively, which obviously had superhydrophilic and superaerophobic properties. Based on the above results, it is shown that the Ti₃C₂-assisted preparation of Ni(OH)₂ nanoarrays can significantly improve the superhydrophilic and superaerophobic properties of the catalytic electrodes. The Pt/TiO₂/Ni(OH)₂/NF displayed excellent performance in both OER and HER tests [Figure 7D and E]. The water electrolysis using the Pt/TiO₂/Ni(OH)₂/NF as the cathode and anode required only 1.83 and 1.95 V to afford large current densities of 500 and 1,000 mA·cm⁻², respectively [Figure 7F]. Furthermore, the Pt/TiO₂/Ni(OH)₂/NF electrodes showed remarkable stability for full water electrolysis at 500 and 1,000 mA·cm⁻² as measured by chronoamperometric (i-t) over 25 h [Figure 7G], realizing stable operation of AWEs at high current densities.

These studies construct electrodes with superhydrophilic and superaerophobic properties, which greatly promote the release of surface bubbles and provide a reliable way for the contact between electrolyte and catalytic active sites; the OER and HER electrochemical performance can also be improved. In future studies, the effects of different electrode surface morphology and wettability on gas kinetics need to be further investigated to reduce the accumulation of bubbles on the electrode surface and improve the efficiency of OER/HER. Additionally, the electrolyte pH should be considered as it affects bubble

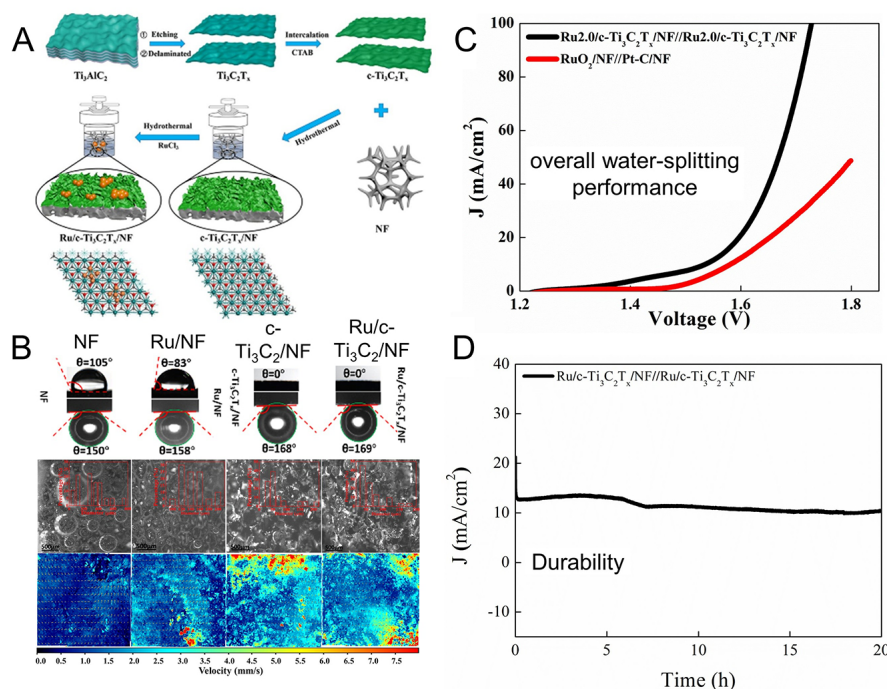


Figure 6. Ru/MXene 3D electrode with superhydrophilicity and superaerophobicity for overall water splitting. (A) the synthesis process of Ru/c-Ti₃C₂T_x/NF electrode; (B) the contact angles of water droplets and underwater contact angles of gas bubbles, the digital images of bubble generation behavior and the corresponding fluid velocity vector field of the electrolyte on NF, Ru/NF, c-Ti₃C₂/NF, and Ru/c-Ti₃C₂/NF electrodes; (C) overall water-splitting performance of Ru/c-Ti₃C₂/NF//Ru/c-Ti₃C₂/NF and RuO₂/NF//Pt-C/NF at 5 mV·s⁻¹ in 1.0 M KOH; (D) durability of Ru/c-Ti₃C₂/NF//Ru/c-Ti₃C₂/NF as demonstrated by chronoamperometry at 10 mA·cm⁻². These figures are quoted with permission from Kong et al.^[68]. NF: Nickel foam.

detachment diameter from electrode surfaces by electrostatic interaction. Alkaline water electrolysis with a higher concentration of KOH or NaOH would reduce the detachment diameter of bubbles, resulting in a shorter residence time at the electrode^[72].

Bipolar plate flow channels

According to different electrode gap conditions, AWEs can be classified as finite-gap electrolyzers, zero-gap electrolyzers, or zero-gap anion-exchange membrane electrolyzers. Traditional finite-gap alkaline electrolysis involves two electrode plates separated by a liquid alkaline electrolyte, which suffers from a low current density (< 250 mA·cm⁻²) and low efficiency (< 60%), mainly because of the high internal resistance losses^[73,74]. In comparison, zero-gap electrolyzers or zero-gap anion-exchange membrane electrolyzers feature a simple diaphragm separating the two electrodes, which thereby minimizes ohmic losses in the electrolyte^[75,76]. A more detailed comparison of different AWEs can be found in Table 2. The bipolar plate supports the electrodes, conducts electrons, and connects adjacent cells in the stack of both zero-gap AWEs and zero-gap alkaline anion-exchange membrane water electrolyzers^[77]. Moreover, its flow channel structure promotes uniform electrolyte distribution in the electrolytic chamber^[78]. Electrolyzer performance can be adversely affected by gas accumulation on electrodes^[45,46]. Proper flow promotes the timely discharge of bubbles from the electrode, and the uniformity of gas phase distributions affects the conductivity of electrolytes^[77]. As a result, designing a flow channel is an extremely important part of electrolyzer design.

Flow channel effects require a detailed study of the multiphase flow field within the electrolyzer, which is not possible with common optical testing techniques because of its hermetic nature. Consequently, multiphase flow and reaction behavior of electrolytic cells have been simulated numerically using

Table 2. Comparison of different alkaline water electrolyzers

	FGE	ZGE	ZGAEME
Distance between diaphragm and electrode (mm)	0.50-20	0	0
Diaphragm materials	-	Porous membrane (asbestos, polyphenylene sulfide, etc.)	Anion-exchange membrane (polybenzimidazole, poly(aryl piperidine), poly(phenylene) oxide, etc.)
Operating temperature (°C)	60-95	60-95	30-60
Current density (A·cm ⁻²)	0.10-0.50	0.15-0.65	1.00-2.00
H ₂ purity (%)	-	99.80-100	99.99-100
Merits	Simple structure	Mature, industrial, low investment	High purity of H ₂ , adaptability to the fluctuation of power supply, safe and pollution-free
Demerits	Low purity, low efficiency	Complex and high cost	Narrow technology of exchange membrane

FGE: Finite-gap electrolyzer; ZGAEME: zero-gap anion exchange membrane electrolyzer; ZGE: zero-gap electrolyzer.

computational fluid dynamics (CFD)^[79,80]. Due to the strong nonlinearity of the Euler-Euler $k-\varepsilon$ turbulence model, the turbulent variables involved in the two-phase flow greatly increase the degrees of freedom of the model. In a more complex three-dimensional electrolyzer structure, the coupling of the Euler-Euler two-phase turbulent field and electric field is more difficult to converge. Thus, little is known about the bipolar plate flow channel structure or the combination of the bipolar plate and electrode in the zero-gap alkaline electrolyzer. Lee *et al.*^[69] and Huang *et al.*^[81] established three-dimensional two-phase zero-gap alkaline water electrolysis models with straight-type [Figure 8A-C] and ring cross-type [Figure 8D-F] flow channel structures, respectively. They evaluated the effects of two-phase flow initiation and bubble coverage. Through the simulations, it was possible to determine the effects of operating parameters, such as voltage, electrolyte flow, and temperature, on gas distributions and current density distributions. There was no attention paid to the effect of change in flow channel structure on electrolysis. In a study by Wong *et al.*, the bubble behavior in a single serpentine flow channel was investigated by simulation, and the flow state around square and rounded bends of a single serpentine flow channel was examined and compared in terms of velocity and pressure drop [Figure 8G-I]^[82]. Due to its smaller low velocity region and higher pressure stability, the rounded bend provided better bubble separation from the electrode than the square bend. According to Wong *et al.*, even small changes in flow channel structure had a large effect on the electrolysis cell flow state^[82]. It is, therefore, very important to optimize the flow channel structure to promote bubble separation, and more in-depth research is necessary to accomplish this.

There are different types of flow channels, each with its advantages and disadvantages. The flow channels of an industrial AWE must be easy to process and capable of handling high pressures and flows. Square column flow channels have grooves formed by protruding square columns that allow the electrolyte to flow through. As a result of this structure, high flow rates are possible in the electrolyzer, resulting in uniform distribution of the electrolyte and efficient transport of bubbles generated in the NF electrodes while having a lower pressure drop^[77]. As a further step toward optimizing this structure, our group evaluated the effects of different square column flow channel structures on the gas distribution and electrolysis performance of an alkaline electrolyzer. Simulating various parameters on the $I-V$ characteristic curve and hydrodynamic characteristics allowed us to determine the optimal structural parameters. As shown in Table 3, sixteen different geometric models of alkaline electrolyzers were constructed, and their representative models were shown in Figure 9A-F. Figure 9G and H show the corresponding boundary conditions and meshing. Parameters considered included flow channel height (h_{ch}), arrangements of square columns, and the number of flow inlets and outlets in the electrolyzer^[83].

Table 3. Size parameters of electrolyzers in different geometric structures^[83]

Structure name	h_ch (mm)	Arrangement of conductive columns	h_w (mm)	w_ch (mm)	Number of inlets/outlets
G-2.5-T-0-3-1	2.5	Triangular	0	3	1
G-2.5-T-0.05-3-1	2.5	Triangular	0.05	3	1
G-2.5-T-1-3-1	2.5	Triangular	1	3	1
G-2.5-T-2-3-1	2.5	Triangular	2	3	1
G-2.25-T-0-3-1	2.25	Triangular	0	3	1
G-3-T-0-3-1	3	Triangular	0	3	1
G-2.5-S-0-3-1	2.5	Square	0	3	1
G-2.5-T-0-3-3	2.5	Triangular	0	3	3
G-2.5-T-0-5-1	2.5	Triangular	0	5	1
G-2.5-S-0-5-1	2.5	Square	0	5	1
G-2.5-S-0-7-1	2.5	Square	0	7	1
G-2.25-T-0-3-3	2.25	Triangular	0	3	3
G-3-T-0-3-3	3	Triangular	0	3	3
G-2.5-T-0-5-3	2.5	Triangular	0	5	3
G-2.5-S-0-5-3	2.5	Square	0	5	3
G-2.5-S-0-7-3	2.5	Square	0	7	3

As shown in [Figure 10A-L](#), by deepening the flow channel, we found that lye distribution is more uniform, and the gas is removed more quickly. This resulted in a lower voltage compared to the electrolyzer with a small flow channel height [[Figure 10M](#)]. After that, the number of flow inlets and outlets and the arrangement of square columns were examined for their impact on electrolyzer performance. There was evidence that triangular channels could result in more uniform gas distributions, which mitigated bubble effects. To combat the inlet circulation issue and uneven fluid distribution resulting from a single inlet and outlet, a multi-port electrolyzer with high flow was used to increase the flow rate in the side chamber, reduce the dead zone in the middle flow field, and lower the cell voltage significantly [[Figure 10N](#)]. It is particularly noticeable at high current densities.

To leverage the advantages of the multi-port design, the channel height and column spacing of the multi-port electrolyzer were further examined. There was a significant impact on the spacing between the conductive columns in multiple inlet and outlet electrolyzers. The normal flow rate refers to the velocity perpendicular to the electrode surface, and its direction is further classified as positive or negative depending on the effect it has on the bubbles. Specifically, the positive direction is defined as the direction in which the electrolyte enters the electrode perpendicular to the electrode surface and squeezes the bubbles. The negative direction is the direction in which the electrode liquid drives the bubbles vertically into the flow channel from the inside of the electrode. The mixture velocity is the combined velocity of the electrolyte in three directions, which drives the electrolyte to bring out bubbles in different directions. It follows that the greater the absolute value of the normal velocity and the mixture velocity of the electrode liquid, the more effective it is at taking out bubbles from the electrode, thus reducing gas occupation of the effective area of electrodes and ensuring normal ion transmission. When this spacing is increased, the central flow rate of the KOH aqueous solution in the channel and the normal flow rate of the electrode surface of the cell could be effectively increased [[Figure 11A-H](#)], reducing bubble effects and lowering cell voltage. Of the various types of electrolyzers, the electrolyzer G-2.5-T-0-5-3 demonstrated the best performance in terms of improving the normal flow rate and reducing the cell voltage [[Figure 11I and J](#)].

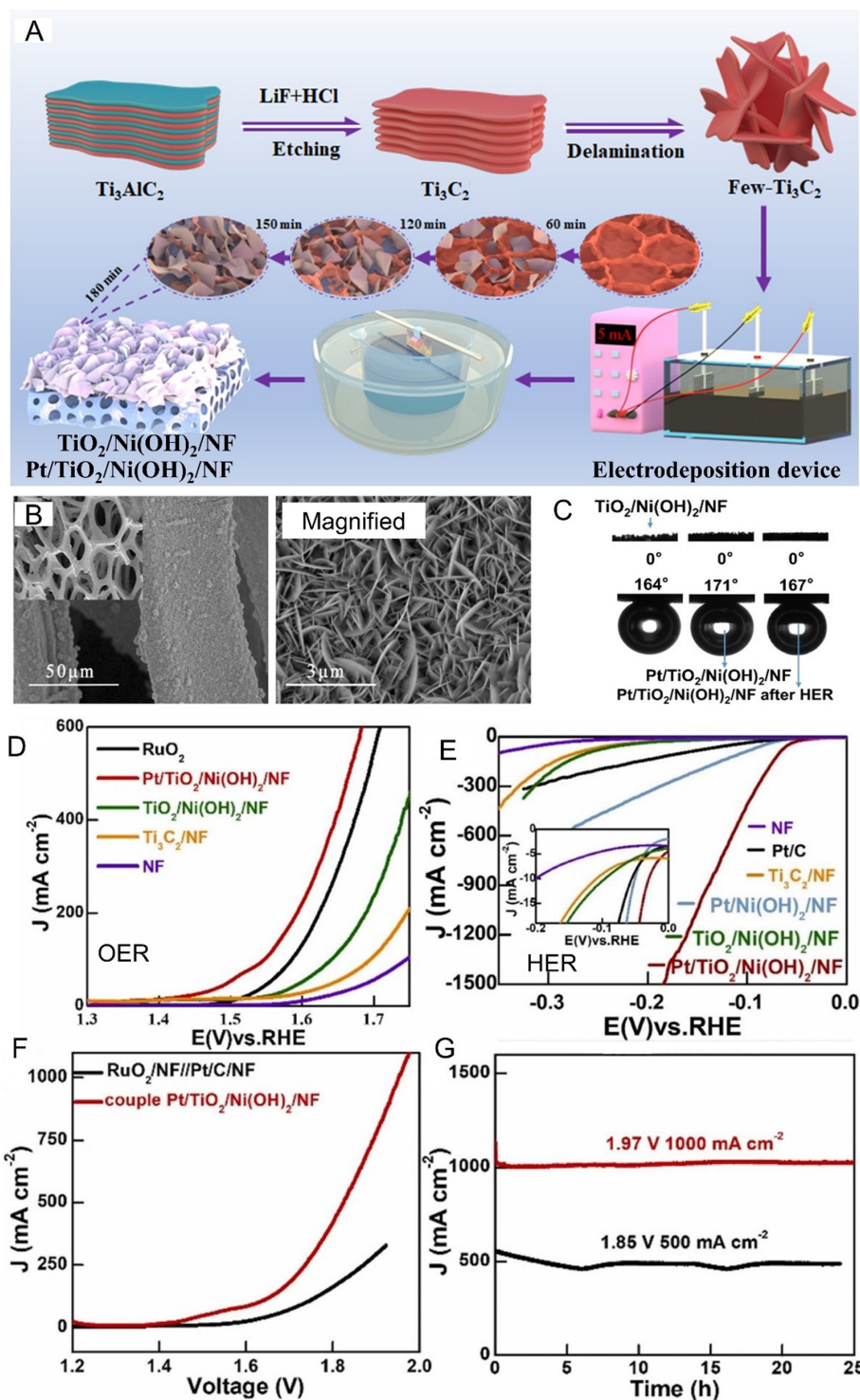


Figure 7. Robust $\text{Pt}/\text{TiO}_2/\text{Ni}(\text{OH})_2$ nanosheet arrays for high current density alkaline water electrolysis. (A) the synthesis process of $\text{Pt}/\text{TiO}_2/\text{Ni}(\text{OH})_2/\text{NF}$ nanosheet arrays and (B) corresponding SEM image; (C) underwater contact angles of water droplets and the contact angles of gas bubbles on $\text{TiO}_2/\text{Ni}(\text{OH})_2/\text{NF}$, $\text{Pt}/\text{TiO}_2/\text{Ni}(\text{OH})_2/\text{NF}$, and $\text{Pt}/\text{TiO}_2\text{-Ni}(\text{OH})_2/\text{NF}$ after the HER stability test, respectively; (D) and (E) OER LSV curves and corresponding Tafel plots for NF, $\text{Ti}_3\text{C}_2/\text{NF}$, $\text{TiO}_2/\text{Ni}(\text{OH})_2/\text{NF}$, RuO_2 , and $\text{Pt}/\text{TiO}_2/\text{Ni}(\text{OH})_2/\text{NF}$; (F) Overall water splitting LSV curves for $\text{Pt}/\text{TiO}_2/\text{Ni}(\text{OH})_2/\text{NF}$ couples and commercial Pt/C and RuO_2 couples; (G) stability test at 500 and 1,000 mA cm^{-2} . These figures are quoted with permission from Kong et al.^[71]. NF: Nickel foam.

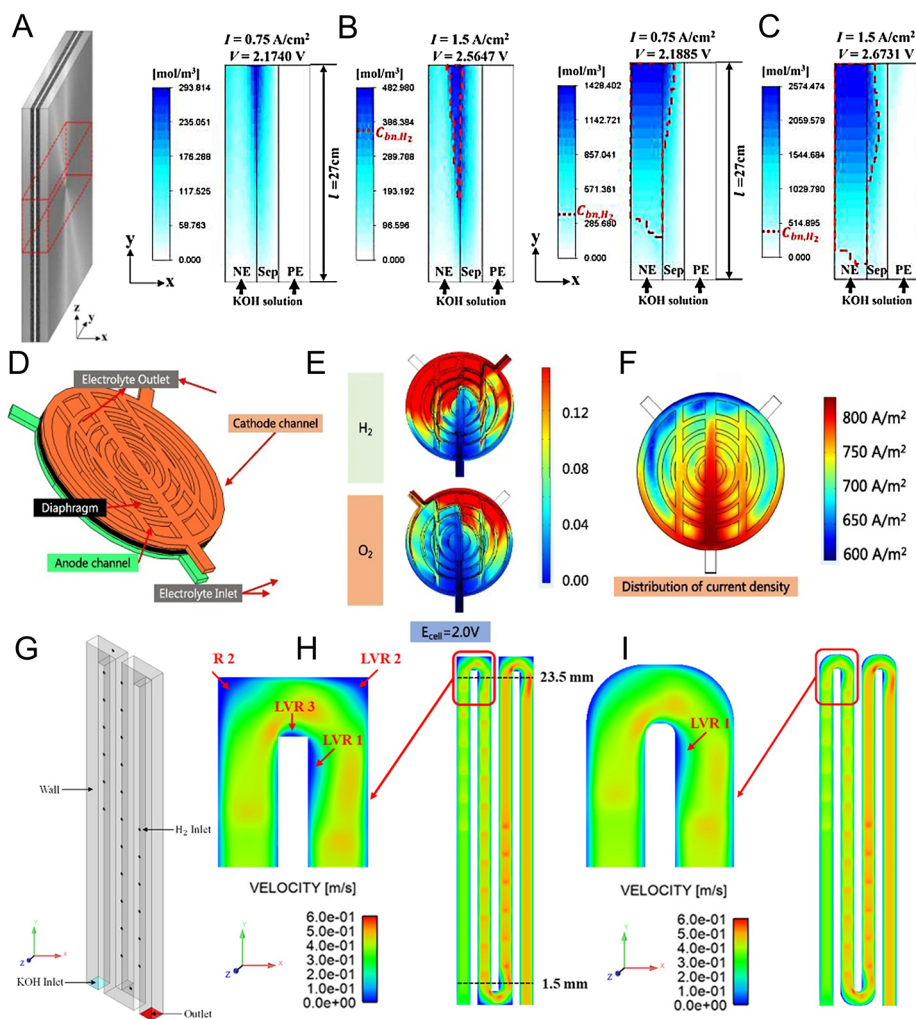


Figure 8. Effects of different flow channel structures on water electrolysis^[69,81,82]. Straight-type flow channel: (A) computational domain and mesh configuration of a zero-gap AWE cell; (B) and (C) contours of H_2/O_2 molar concentration over the plane cutting across the center at $v_{in} = 0.1 \text{ m/s}$. These figures are quoted with permission from Lee *et al.*^[69]. Ring cross-type flow channel: (D) three-dimensional structure of the electrolyzer cell; (E) distribution of hydrogen and oxygen in the flow channel of anode and cathode; (F) the uneven distribution of current densities of the catalyst due to the bubble effect ($E_{cell} = 2.1 \text{ V}$). These figures are quoted with permission from Huang *et al.*^[81]. Single serpentine flow channel: (G) geometry and boundary conditions of the computational domain; the flow state around square (H) and rounded (I) bends. These figures are quoted with permission from Wong *et al.*^[82]. AWE: Alkaline water electrolyzer.

The electrolyzers with conductive columns shown above demonstrated that a multi-port electrolyzer with wide spacing between conductive columns could enhance rapid bubble detachment and reduce alkaline water electrolysis voltage requirements. Future studies should investigate the scaling-up effects of different flow channel structures to provide more reliable and economical model design tools for alkaline water electrolysis.

CONCLUSION AND OUTLOOK

This review provides a comprehensive overview of various techniques for improving bubble separation in AWEs, which, to our knowledge, is the first comprehensive examination of these techniques. It first examines the negative effects of bubbles inside AWEs. Afterward, recent progress on improving bubble separation is discussed in detail. Specifically, it can be divided into two categories: external operation

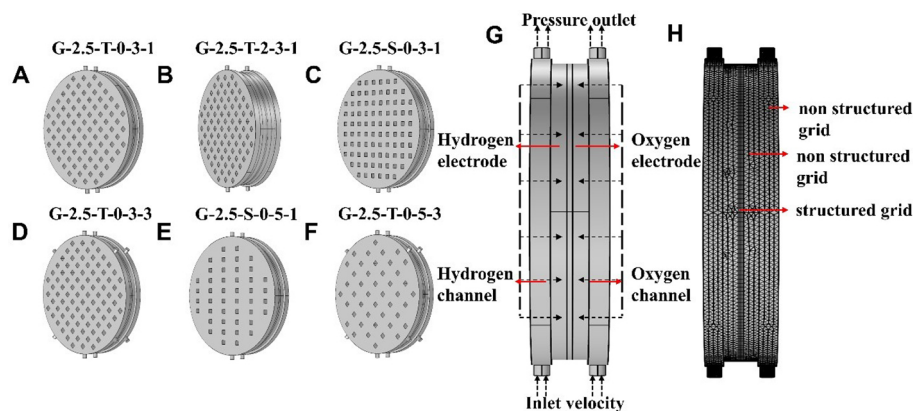


Figure 9. Construction of a representative geometric model of alkaline electrolyzers. (A) G-2.5-T-0-3-1; (B) G-2.5-T-2-3-1; (C) G-2.5-S-0-3-1; (D) G-2.5-T-0-3-3; (E) G-2.5-S-0-5-1; (F) G-2.5-T-0-5-3; (G) boundary condition settings; (H) meshing. This figure is quoted with permission from Gao et al.^[83].

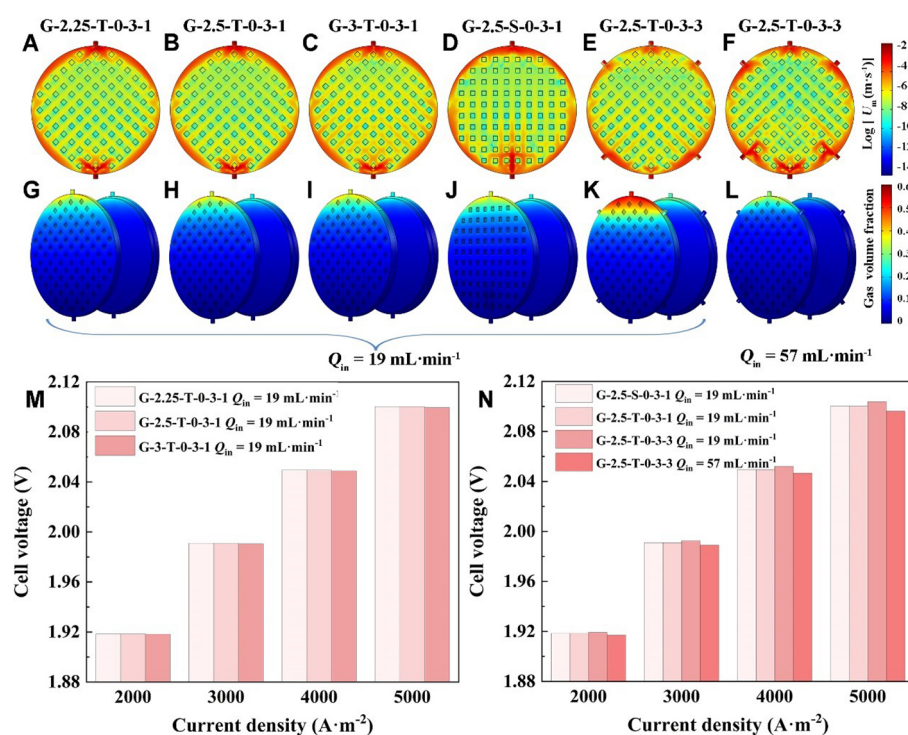


Figure 10. Effects of structural parameters on the performance of alkaline electrolyzer. (A) mixture velocity of G-2.25-T-0-3-1; (B) mixture velocity of G-2.5-T-0-3-1; (C) mixture velocity of G-3-T-0-3-1; (D) mixture velocity of G-2.5-S-0-3-1; (E) mixture velocity of G-2.5-T-0-3-3; (F) mixture velocity of G-2.5-T-0-3-3; (G) gas volume fraction of G-2.25-T-0-3-1; (H) gas volume fraction of G-2.5-T-0-3-1; (I) gas volume fraction of G-3-T-0-3-1; (J) gas volume fraction of G-2.5-S-0-3-1; (K) gas volume fraction of G-2.5-T-0-3-3; (L) gas volume fraction of G-2.5-T-0-3-3; (M) cell voltage of different channel heights; (N) cell voltage of different numbers of flow inlets and outlets. This figure is quoted with permission from Gao et al.^[83].

enhancements (such as applying external fields, flow operation, fluctuation operations, and adding surfactants to the electrolyte) and internal optimizations of key structures (such as the electrodes and bipolar plate flow channels). It is worth noting that the latest results of our group are presented regarding the novel electrode structure and various bipolar plate flow channel structures. Additionally, the advantages and disadvantages of various strengthening methods used in industrial electrolyzers are analyzed from the

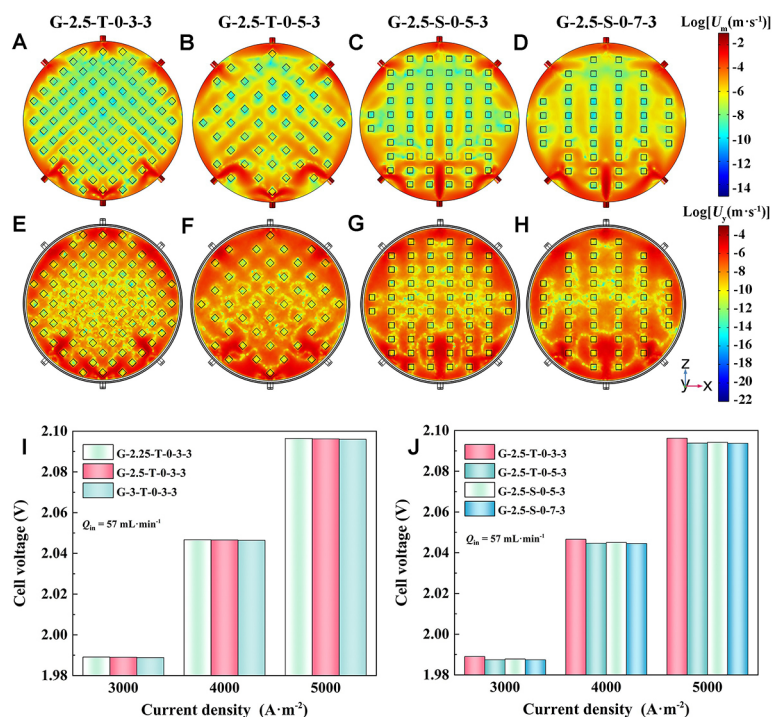


Figure 11. Effects of channel height and column spacing on the performance of multi-port electrolyzers. (A) mixture velocity of G-2.5-T-0-3-3; (B) mixture velocity of G-2.5-T-0-5-3; (C) mixture velocity of G-2.5-S-0-5-3; (D) mixture velocity of G-2.5-S-0-7-3; (E) normal velocity of electrode surface of G-2.5-T-0-3-3; (F) normal velocity of electrode surface of G-2.5-T-0-5-3; (G) normal velocity of electrode surface of G-2.5-S-0-5-3; (H) normal velocity of electrode surface of G-2.5-S-0-7-3; (I) cell voltage of multi-port electrolyzers under different channel heights; (J) cell voltage of multi-port electrolyzers under different column spacings. This figure is quoted with permission from Gao et al.^[83].

standpoint of their application in industry. These advancements provide high-performance electrodes and optimal flow channel structures for alkaline water electrolysis, addressing flow rate distribution, gas distribution, and voltage characteristics.

Clearly, progress is being made in bubble separation, but challenges remain. In order to reduce the negative effects of bubbles and make alkaline water electrolysis cost-effective and energy-saving, the following directions warrant investigation. For instance, the main focus of most researchers at present is on adjusting the wettability of electrode surfaces and designing electrode structures to separate bubbles from electrode surfaces. Nevertheless, bubbles are generated preferentially in the pores or uneven areas of the electrode surface, and the nucleation sites are specific. Observing how bubbles form on electrode surfaces would help separate bubbles by removing them from easily accessible locations. Alternatively, capillaries could produce hydrogen from alkaline water by delivering KOH solution to the porous electrode surface without producing bubbles. Also, the flow channel structure, especially for large-scale AWEs, should be studied in detail and rationally designed. There has not been much exploration of this front, which may be a promising direction for future research. By exploring these directions, researchers can further improve the efficiency and effectiveness of alkaline water electrolysis and address the challenges associated with bubble separation.

DECLARATIONS

Authors' contributions

Collected and analyzed relevant literature, wrote the draft, and designed figures: Yang L, Gao L, Shan G, Huo X, Zhang M, Wang Y, Liu X, Kong A

Conceptualized and led the project, directed the writing, and modified the manuscript: Zhang J, Wu J

Availability of data and materials

Not applicable.

Financial support and sponsorship

The work was supported by the National Key Research and Development Program of China (No. 2021YFB4000303) and the National Natural Science Foundation of China (No. 22090034).

Conflicts of interest

All authors declared that there are no conflicts of interest.

Ethical approval and consent to participate

Not applicable.

Consent for publication

Not applicable.

Copyright

© The Author(s) 2023.

REFERENCES

1. Holladay J, Hu J, King D, Wang Y. An overview of hydrogen production technologies. *Catal Today* 2009;139:244-60. [DOI](#)
2. Turner JA. Sustainable hydrogen production. *Science* 2004;305:972-4. [DOI](#) [PubMed](#)
3. Buttler A, Spliethoff H. Current status of water electrolysis for energy storage, grid balancing and sector coupling via power-to-gas and power-to-liquids: a review. *Renew Sustain Energy Rev* 2018;82:2440-54. [DOI](#)
4. Xie WF, Shao MF. Alkaline water electrolysis for efficient hydrogen production. *J Electrochem* 2022;28:22014008. [DOI](#)
5. Schmidt O, Gambhir A, Staffell I, Hawkes A, Nelson J, Few S. Future cost and performance of water electrolysis: an expert elicitation study. *Int J Hydrog Energy* 2017;42:30470-92. [DOI](#)
6. Yu ZY, Duan Y, Feng XY, Yu X, Gao MR, Yu SH. Clean and affordable hydrogen fuel from alkaline water splitting: past, recent progress, and future prospects. *Adv Mater* 2021;33:e2007100. [DOI](#) [PubMed](#)
7. Zouhri K, Lee S. Evaluation and optimization of the alkaline water electrolysis ohmic polarization: exergy study. *Int J Hydrog Energy* 2016;41:7253-63. [DOI](#)
8. Zeng K, Zhang D. Recent progress in alkaline water electrolysis for hydrogen production and applications. *Prog Energy Combust Sci* 2010;36:307-26. [DOI](#)
9. Wang M, Wang Z, Gong X, Guo Z. The intensification technologies to water electrolysis for hydrogen production - a review. *Renew Sustain Energy Rev* 2014;29:573-88. [DOI](#)
10. Yin W, Cai Y, Xie L, et al. Revisited electrochemical gas evolution reactions from the perspective of gas bubbles. *Nano Res* 2023;16:4381-98. [DOI](#)
11. Zhao X, Ren H, Luo L. Gas Bubbles in electrochemical gas evolution reactions. *Langmuir* 2019;35:5392-408. [DOI](#)
12. Angulo A, van der Linde P, Gardeniers H, Modestino M, Fernández Rivas D. Influence of bubbles on the energy conversion efficiency of electrochemical reactors. *Joule* 2020;4:555-79. [DOI](#)
13. Deng X, Yang F, Li Y, Dang J, Ouyang M. Quantitative study on gas evolution effects under large current density in zero-gap alkaline water electrolyzers. *J Power Sources* 2023;555:232378. [DOI](#)
14. Lu Z, Li Y, Lei X, Liu J, Sun X. Nanoarray based "superaerophobic" surfaces for gas evolution reaction electrodes. *Mater Horiz* 2015;2:294-8. [DOI](#)
15. Weijts MPMG, Janssen LJJ, Visser GJ. Ohmic resistance of solution in a vertical gas-evolving cell. *J Appl Electrochem* 1997;27:371-8. [DOI](#)
16. Xie Y, Zhang LY, Ying PJ, Wang JC, Sun K, Li M. Intensified field-effect of hydrogen evolution reaction. *Prog Chem* 2021;33:1571-85. [DOI](#)
17. Weier T, Baczymalski D, Massing J, Landgraf S, Cierpka C. The effect of a lorentz-force-driven rotating flow on the detachment of gas bubbles from the electrode surface. *Int J Hydrog Energy* 2017;42:20923-33. [DOI](#)
18. Martin M. Bi'āñki's ghost dance map: thanatoptic cartography and the native american spirit world. *Imago Mundi* 2013;65:106-14. [DOI](#)

19. Liu Y, Pan L, Liu H, Chen T, Yin S, Liu M. Effects of magnetic field on water electrolysis using foam electrodes. *Int J Hydrog Energy* 2019;44:1352-8. DOI
20. Niether C, Faure S, Bordet A, et al. Improved water electrolysis using magnetic heating of FeC-Ni core-shell nanoparticles. *Nat Energy* 2018;3:476-83. DOI
21. Garcés-pineda FA, Blasco-ahicart M, Nieto-castro D, López N, Galán-mascarós JR. Direct magnetic enhancement of electrocatalytic water oxidation in alkaline media. *Nat Energy* 2019;4:519-25. DOI
22. Wang M, Wang Z, Guo Z. Understanding of the intensified effect of super gravity on hydrogen evolution reaction. *Int J Hydrog Energy* 2009;34:5311-7. DOI
23. Wang M, Wang Z, Guo Z. Water electrolysis enhanced by super gravity field for hydrogen production. *Int J Hydrog Energy* 2010;35:3198-205. DOI
24. Rashwan SS, Dincer I, Mohany A. A review on the importance of operating conditions and process parameters in sonic hydrogen production. *Int J Hydrog Energy* 2021;46:28418-34. DOI
25. Cho KM, Deshmukh PR, Shin WG. Hydrodynamic behavior of bubbles at gas-evolving electrode in ultrasonic field during water electrolysis. *Ultrason Sonochem* 2021;80:105796. DOI PubMed PMC
26. Li S, Wang C, Chen C. Water electrolysis in the presence of an ultrasonic field. *Electrochim Acta* 2009;54:3877-83. DOI
27. Madigan NA, Hagan CR, Zhang H, Coury LA. Effects of sonication on electrode surfaces and metal particles. *Ultrason Sonochem* 1996;3:S239-47. DOI
28. Swiegers GF, Terrett RNL, Tsekouras G, Tsuzuki T, Pace RJ, Stranger R. The prospects of developing a highly energy-efficient water electrolyser by eliminating or mitigating bubble effects. *Sustain Energy Fuels* 2021;5:1280-310. DOI
29. Sullivan I, Zhang H, Zhu C, et al. 3D printed nickel-molybdenum-based electrocatalysts for hydrogen evolution at low overpotentials in a flow-through configuration. *ACS Appl Mater Interfaces* 2021;13:20260-8. DOI
30. Chen Y, Chen J, Bai K, Xiao Z, Fan S. A flow-through electrode for hydrogen production from water splitting by mitigating bubble induced overpotential. *J Power Sources* 2023;561:232733. DOI
31. Bakker MM, Vermaas DA. Gas bubble removal in alkaline water electrolysis with utilization of pressure swings. *Electrochim Acta* 2019;319:148-57. DOI
32. Monk N, Watson S. Review of pulsed power for efficient hydrogen production. *Int J Hydrog Energy* 2016;41:7782-91. DOI
33. Demir N, Kaya MF, Albawabiji MS. Effect of pulse potential on alkaline water electrolysis performance. *Int J Hydrog Energy* 2018;43:17013-20. DOI
34. Hosseini SR, Ghasemi S, Ghasemi SA. Effect of surfactants on electrocatalytic performance of copper nanoparticles for hydrogen evolution reaction. *J Mol Liq* 2016;222:1068-75. DOI
35. Wei Z, Ji M, Chen S, et al. Water electrolysis on carbon electrodes enhanced by surfactant. *Electrochim Acta* 2007;52:3323-9. DOI
36. Brinkert K, Richter MH, Akay Ö, et al. Efficient solar hydrogen generation in microgravity environment. *Nat Commun* 2018;9:2527. DOI PubMed PMC
37. Browne MP, Vasconcelos JM, Coelho J, et al. Improving the performance of porous nickel foam for water oxidation using hydrothermally prepared Ni and Fe metal oxides. *Sustain Energy Fuels* 2017;1:207-16. DOI
38. Li S, Xie W, Song Y, et al. Integrated CoPt electrocatalyst combined with upgrading anodic reaction to boost hydrogen evolution reaction. *Chem Eng J* 2022;437:135473. DOI
39. Wang C, Jiang X, Wang Y, Tang Y, Zhou J, Fu G. Recent advances in nonmetallic modulation of palladium-based electrocatalysts. *Chem Synth* 2023;3:8. DOI
40. Cong Y, Mccrum IT, Gao X, et al. Uniform Pd_{0.33}Ir_{0.67} nanoparticles supported on nitrogen-doped carbon with remarkable activity toward the alkaline hydrogen oxidation reaction. *J Mater Chem A* 2019;7:3161-9. DOI
41. Wang X, Zhang L, Liu CP, Ge JJ, Zhu JB, Xing W. Recent advances in structural regulation on non-precious metal catalysts for oxygen reduction reaction in alkaline electrolytes. *J Electrochem* 2022;28:2108501. DOI
42. Yang F, Kim MJ, Brown M, Wiley BJ. Alkaline Water Electrolysis at 25 A cm⁻² with a microfibrillar flow-through electrode. *Adv Energ Mater* 2020;10:2001174. DOI
43. Schalenbach M, Kasian O, Mayrhofer KJ. An alkaline water electrolyzer with nickel electrodes enables efficient high current density operation. *Int J Hydrog Energy* 2018;43:11932-8. DOI
44. Phillips R, Edwards A, Rome B, Jones DR, Dunnill CW. Minimising the ohmic resistance of an alkaline electrolysis cell through effective cell design. *Int J Hydrog Energy* 2017;42:23986-94. DOI
45. Alexiadis A, Dudukovic M, Ramachandran P, Cornell A, Wanggård J, Bokkers A. Liquid-gas flow patterns in a narrow electrochemical channel. *Chem Eng Sci* 2011;66:2252-60. DOI
46. de Groot MT, Vreman AW. Ohmic resistance in zero gap alkaline electrolysis with a Zirfon diaphragm. *Electrochim Acta* 2021;369:137684. DOI
47. Kim J, Lee J, Yoo C, Lee K, Lee W. Low-cost and energy-efficient asymmetric nickel electrode for alkaline water electrolysis. *Int J Hydrog Energy* 2015;40:10720-5. DOI
48. Paul MT, Yee BB, Bruce DR, Gates BD. Hexagonal arrays of cylindrical nickel microstructures for improved oxygen evolution reaction. *ACS Appl Mater Interfaces* 2017;9:7036-43. DOI PubMed
49. Fujimura T, Kunimoto M, Fukunaka Y, Homma T. Analysis of the hydrogen evolution reaction at Ni micro-patterned electrodes. *Electrochim Acta* 2021;368:137678. DOI

50. Iwata R, Zhang L, Wilke KL, et al. Bubble growth and departure modes on wettable/non-wettable porous foams in alkaline water splitting. *Joule* 2021;5:887-900. DOI
51. Teschke O, Galembeck F. Effect of PTFE coverage on the performance of gas evolving electrodes. *J Electrochem Soc* 1984;131:1095-7. DOI
52. Raman A, Peñas P, van der Meer D, Lohse D, Gardeniens H, Fernández Rivas D. Potential response of single successive constant-current-driven electrolytic hydrogen bubbles spatially separated from the electrode. *Electrochim Acta* 2022;425:140691. DOI
53. Li N, Huang C, Wang X, Feng Y, An J. Electrosynthesis of hydrogen peroxide via two-electron oxygen reduction reaction: a critical review focus on hydrophilicity/hydrophobicity of carbonaceous electrode. *Chem Eng J* 2022;450:138246. DOI
54. Garcia-rodriguez O, Lee YY, Olvera-vargas H, Deng F, Wang Z, Lefebvre O. Mineralization of electronic wastewater by electro-Fenton with an enhanced graphene-based gas diffusion cathode. *Electrochim Acta* 2018;276:12-20. DOI
55. Hou D, Jassby D, Nerenberg R, Ren ZJ. Hydrophobic gas transfer membranes for wastewater treatment and resource recovery. *Environ Sci Technol* 2019;53:11618-35. DOI PubMed
56. Forner-Cuenca A, Biesdorf J, Gubler L, Kristiansen PM, Schmidt TJ, Boillat P. Engineered water highways in fuel cells: radiation grafting of gas diffusion layers. *Adv Mater* 2015;27:6317-22. DOI PubMed
57. Hu X, Wang R, Feng W, Xu C, Wei Z. Electrocatalytic oxygen evolution activities of metal chalcogenides and phosphides: fundamentals, origins, and future strategies. *J Energ Chem* 2023;81:167-91. DOI
58. Guo D, Yu H, Chi J, Zhao Y, Shao Z. Cu₂S@NiFe layered double hydroxides nanosheets hollow nanorod arrays self-supported oxygen evolution reaction electrode for efficient anion exchange membrane water electrolyzer. *Int J Hydrog Energy* 2023;48:17743-57. DOI
59. Guo D, Chi J, Yu H, Jiang G, Shao Z. Self-supporting NiFe layered double hydroxide “nanoflower” cluster anode electrode for an efficient alkaline anion exchange membrane water electrolyzer. *Energies* 2022;15:4645. DOI
60. Lu Z, Zhu W, Yu X, et al. Ultrahigh hydrogen evolution performance of under-water “superaerophobic” MoS₂ nanostructured electrodes. *Adv Mater* 2014;26:2683-7. DOI
61. Xu W, Lu Z, Sun X, Jiang L, Duan X. Superwetting electrodes for gas-involving electrocatalysis. *Acc Chem Res* 2018;51:1590-8. DOI PubMed
62. Cheng C, Deng M, Li L, Wei Z. The contribution of water molecules to the hydrogen evolution reaction. *Sci China Chem* 2022;65:1854-66. DOI
63. Tang Y, Yang C, Xu X, et al. MXene Nanoarchitectonics: defect-engineered 2D MXenes towards enhanced electrochemical water splitting. *Adv Energ Mater* 2022;12:2103867. DOI
64. Li S, Li E, An X, Hao X, Jiang Z, Guan G. Transition metal-based catalysts for electrochemical water splitting at high current density: current status and perspectives. *Nanoscale* 2021;13:12788-817. DOI
65. Li Z, Hu R, Song J, et al. Gas-liquid-solid triphase interfacial chemical reactions associated with gas wettability. *Adv Materials Inter* 2021;8:2001636. DOI
66. Andaveh R, Barati Darband G, Maleki M, Sabour Rouhaghdam A. Superaerophobic/superhydrophilic surfaces as advanced electrocatalysts for the hydrogen evolution reaction: a comprehensive review. *J Mater Chem A* 2022;10:5147-73. DOI
67. Shan X, Liu J, Mu H, et al. An engineered superhydrophilic/superaerophobic electrocatalyst composed of the supported CoMoS_x chalcogen for overall water splitting. *Angew Chem Int Ed Engl* 2020;59:1659-65. DOI
68. Kong A, Peng M, Gu H, et al. Synergetic control of Ru/MXene 3D electrode with superhydrophilicity and superaerophobicity for overall water splitting. *Chem Eng J* 2021;426:131234. DOI
69. Lee J, Alam A, Park C, Yoon S, Ju H. Modeling of gas evolution processes in porous electrodes of zero-gap alkaline water electrolysis cells. *Fuel* 2022;315:123273. DOI
70. Kale MB, Borse RA, Goma Abdelkader Mohamed A, Wang Y. Electrocatalysts by electrodeposition: recent advances, synthesis methods, and applications in energy conversion. *Adv Funct Mater* 2021;31:2101313. DOI
71. Kong A, Peng M, Liu M, et al. Robust Pt/TiO₂/Ni(OH)₂ nanosheet arrays enable outstanding performance for high current density alkaline water electrolysis. *Appl Catal B Environ* 2022;316:121654. DOI
72. Zhang D, Zeng K. Evaluating the behavior of electrolytic gas bubbles and their effect on the cell voltage in alkaline water electrolysis. *Ind Eng Chem Res* 2012;51:13825-32. DOI
73. Dunnill CW, Rearden A, Mandale S, Glover K, Phillips R. Optimizing the design of an alkaline water splitting device test cell for renewable energy storage as hydrogen. *Arch Chem Chem Eng* 2020;2:1-9. DOI
74. Charles W Dunnill GP, Dunnill C. Water Splitting test cell for renewable energy storage as hydrogen gas. *J Fundam Renew Energy Appl* 2015;5:188. Available from: <https://cronfa.swan.ac.uk/Record/cronfa29225>. [Last accessed on 25 Sep 2023]
75. David M, Ocampo-martinez C, Sánchez-peña R. Advances in alkaline water electrolyzers: a review. *J Energy Storage* 2019;23:392-403. DOI
76. Phillips R, Dunnill C. Zero gap alkaline electrolysis cell design for renewable energy storage as hydrogen gas. *RSC Adv* 2016;6:100643-51. DOI
77. Teuku H, Alshami I, Goh J, Masdar MS, Loh KS. Review on bipolar plates for low-temperature polymer electrolyte membrane water electrolyzer. *Int J of Energy Res* 2021;45:20583-600. DOI
78. Wang J, Wang W, Wang C, Mao Z. Corrosion behavior of three bipolar plate materials in simulated SPE water electrolysis environment. *Int J Hydrog Energy* 2012;37:12069-73. DOI

79. Dominici G, Gabriel B. Analytical study of over-voltages in alkaline electrolysis and their parametric dependencies through a multi-physical model. *Intl J of Energy Res* 2022;46:3295-323. [DOI](#)
80. Jang D, Cho H, Kang S. Numerical modeling and analysis of the effect of pressure on the performance of an alkaline water electrolysis system. *Appl Energy* 2021;287:116554. [DOI](#)
81. Huang D, Xiong B, Fang J, et al. A multiphysics model of the compactly-assembled industrial alkaline water electrolysis cell. *Appl Energy* 2022;314:118987. [DOI](#)
82. Wong XY, Zhuo Y, Shen Y. Numerical analysis of hydrogen bubble behavior in a zero-gap alkaline water electrolyzer flow channel. *Ind Eng Chem Res* 2021;60:12429-46. [DOI](#)
83. Gao L, Yang L, Wang C, et al. Three-dimensional two-phase CFD simulation of alkaline electrolyzers. *J Electrochem* 2023. [DOI](#)